

## **ELECTRONIC SUPPLEMENTARY INFORMATION**

# Photo-induced linkage isomerization in the gas phase probed by tandem ion mobility and laser spectroscopy

*Chang Min Choi,<sup>a</sup> Luke MacAleese,<sup>b</sup> Philippe Dugourd,<sup>b</sup> Myoung Choul Choi,<sup>a</sup> Fabien Chirof<sup>c</sup>*

<sup>a</sup> Mass Spectrometry and Advanced Instrumentation Research Group, Div. of Scientific Instrumentation, Korea Basic Science Institute, Cheongju, Republic of Korea.

<sup>b</sup> Univ Lyon, Université Claude Bernard Lyon 1, CNRS, Institut Lumière Matière UMR 5306, F-69100, Villeurbanne, France.

<sup>c</sup> Univ Lyon, Université Claude Bernard Lyon 1, Ens de Lyon, CNRS, Institut des Sciences Analytiques UMR 5280, 5 rue de la Doua, F-69100, Villeurbanne, France.

## Contents

**Table S 1.** Experimental CCS.

**Table S 2.** CCS simulated from modelled structures.

**Figure S- 1.** Experimental arrival time distributions.

**Figure S- 2.** IMS-resolved photo-fragmentation: photo-fragments ATDs, and mass spectra.

**Figure S- 3.** Power-dependent photo-fragmentation yield at 420 nm.

**Figure S- 4.** Time-dependent solution absorption spectra upon UV irradiation.

**Figure S- 5.** ATDs resulting from collision activation after isomer selection.

**Figure S- 6.** Mass spectra recorded after collisional activation of IMS-selected ions.

**Figure S- 7.** Mass spectra recorded for mass-selected  $[\text{Ru}(\text{bpy})_2(\text{DMSO})]^{2+}$  at different buffer gas flows in the collision cell.

**Figure S- 8.** Relative intensities of the different products of the collisional activation of mass- and ion mobility-selected ions.

**Figure S- 9.** Photo-isomerization spectrum recorded for ion mobility selected  $[\text{Ru}(\text{bpy})_2(\text{DMSO})]^{2+}$  ions.

Isomer designation	Exp <sup>DT</sup> CCS <sub>He</sub> (Å <sup>2</sup> )
SS	139
SO	145
OO	152

**Table S 1.** Collision cross sections measured for the different ion populations identified for  $[\text{Ru}(\text{bpy})_2(\text{DMSO})_2]^{2+}$  ions. The error on the measured values is inferior to 2%.

Isomer designation	<sup>TM</sup> CCS <sub>He</sub> (Å <sup>2</sup> )	MPWB1K/BS2 Energy (kJ.mol <sup>-1</sup> )
cis-OO-GS	152	0
cis-SO-GS	142	3,6
cis-SS-GS	136	30,1

**Table S 2.** Collision cross sections calculated using Jarrold's trajectory method<sup>1</sup> for the ground states structures calculated for the different linkage binding isomers of *cis*- $[\text{Ru}(\text{bpy})_2(\text{DMSO})_2]^{2+}$  ions, together with their relative energies (without solvent), taken from ref. <sup>2</sup>. The standard deviation on the computed values are 3% from the numerical integration procedure.

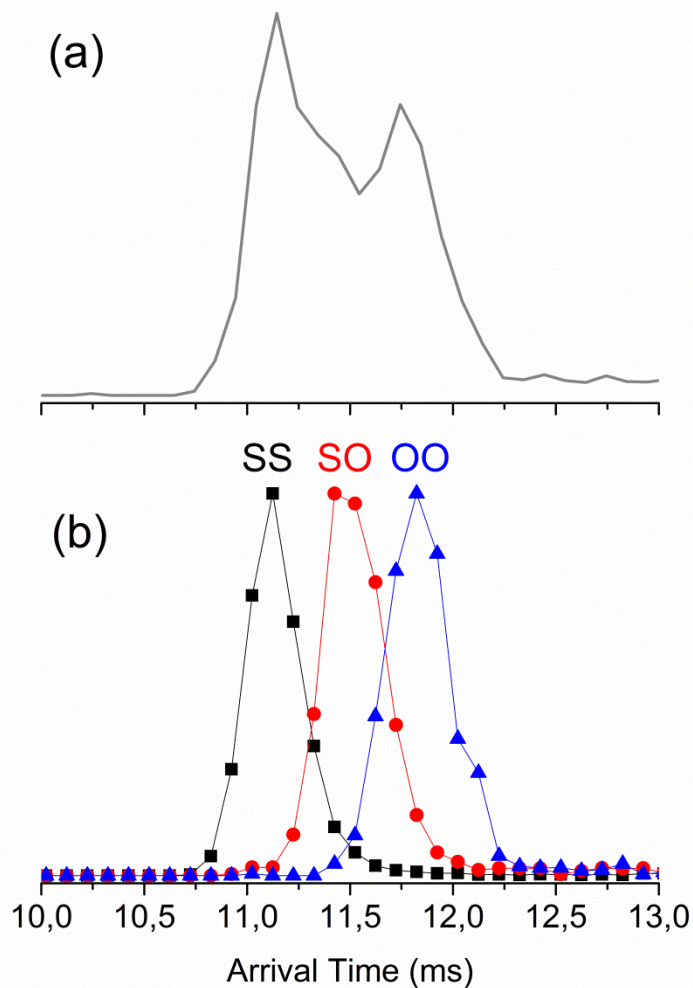


**Figure S- 1.** Arrival time distributions recorded for  $[\text{Ru}(\text{bpy})_2(\text{DMSO})_2]^{2+}$  ions ( $m/z$  285) without selection (a), and (b) after selecting each of the different ion populations, (black squares, red circles, and blue triangles). Each peak is labelled corresponding to the assigned isomer SS, SO, or OO. The drift conditions were identical in both drift tubes: He at 4.0 Torr and 298 K, drift voltage 500 V, drift tube length 0.79 m. The duration of the injection gate was set to 200  $\mu\text{s}$ , and the selection window was 500  $\mu\text{s}$  long.

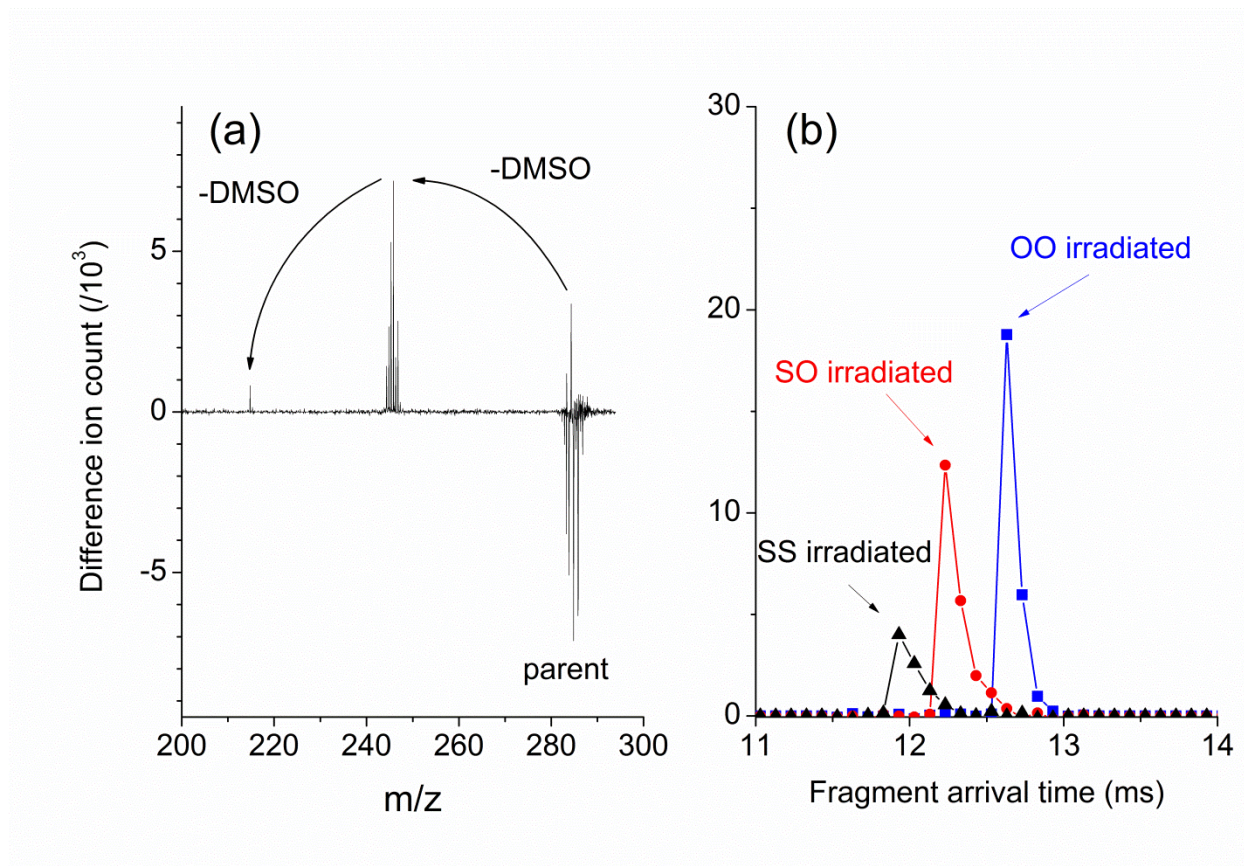


**Figure S- 2.** (a) Difference mass spectrum of the ions detected with and without laser irradiation at 425 nm of mass selected  $[\text{Ru}(\text{bpy})_2(\text{DMSO})_2]^{2+}$  ions. The fragment ions are detected at the arrival time of the irradiated  $[\text{Ru}(\text{bpy})_2(\text{DMSO})_2]^{2+}$  precursor. (b) ATDs of the photo-fragment ions ( $[\text{Ru}(\text{bpy})_2(\text{DMSO})]^{2+}$  and  $[\text{Ru}(\text{bpy})_2]^{2+}$ ) from mobility-separated  $[\text{Ru}(\text{bpy})_2(\text{DMSO})_2]^{2+}$  ions irradiated at 425 nm. The black, red, and blue traces were obtained for different irradiation delays, corresponding to the drift time of the isomers SS, SO, and OO, respectively. The drift time of each fragment is the same as that of its parent.



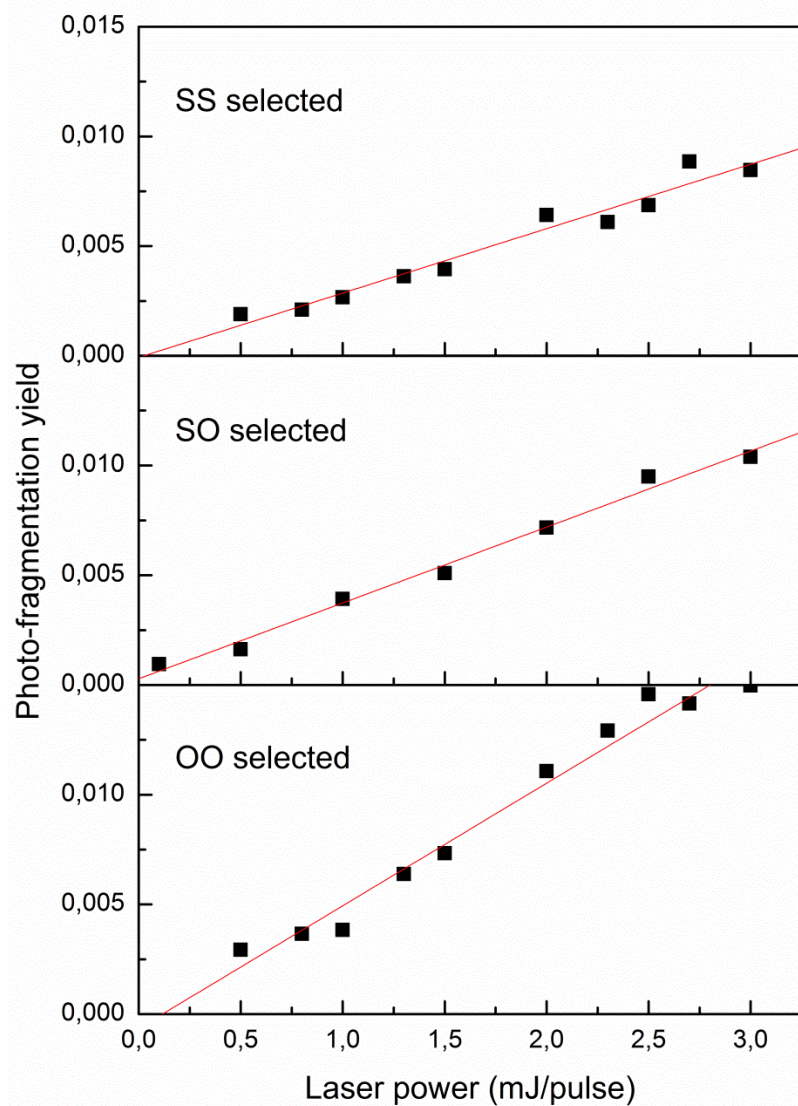


**Figure S- 3.** Photo-fragmentation yield (before power normalization) recorded at 420 nm using different laser powers for ion mobility selected  $[\text{Ru}(\text{bpy})_2(\text{DMSO})_2]^{2+}$  ions corresponding to the different identified linkage isomers (black squares). The red line represents a linear fit of the data.

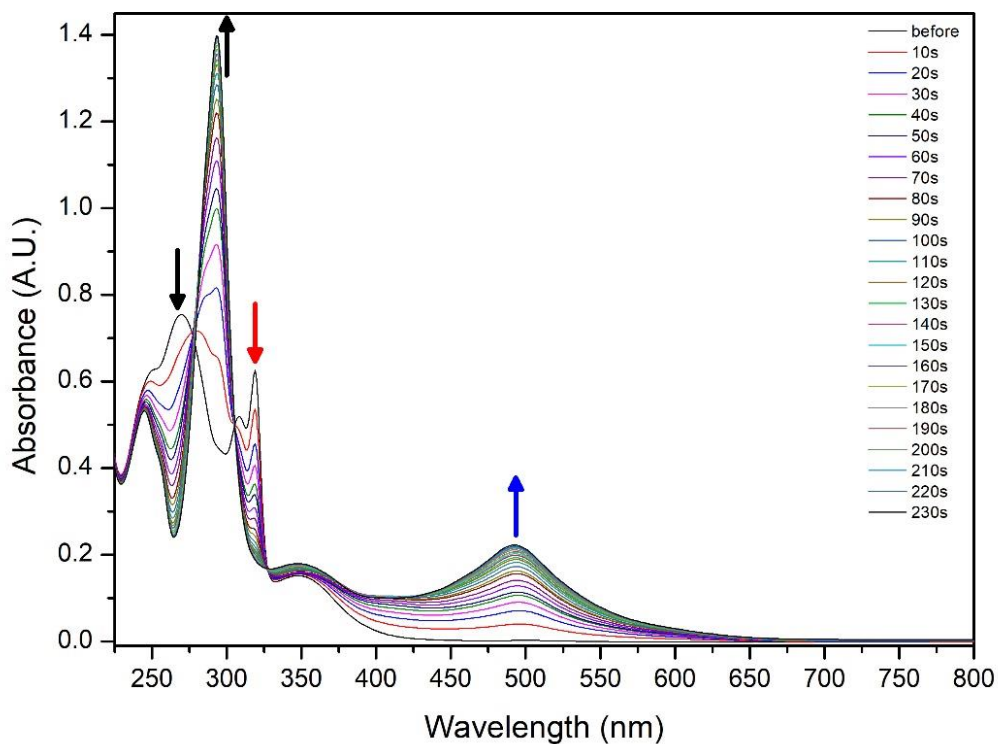


**Figure S- 4.** Time-dependent absorption spectra recorded during UV irradiation of a solution of  $[\text{Ru}(\text{bpy})_2(\text{DMSO})_2]^{2+}$  at  $10 \mu\text{mol.L}^{-1}$  in methanol. The peak rising at about 480 nm was interpreted as the signature of linkage isomerization.<sup>3</sup>

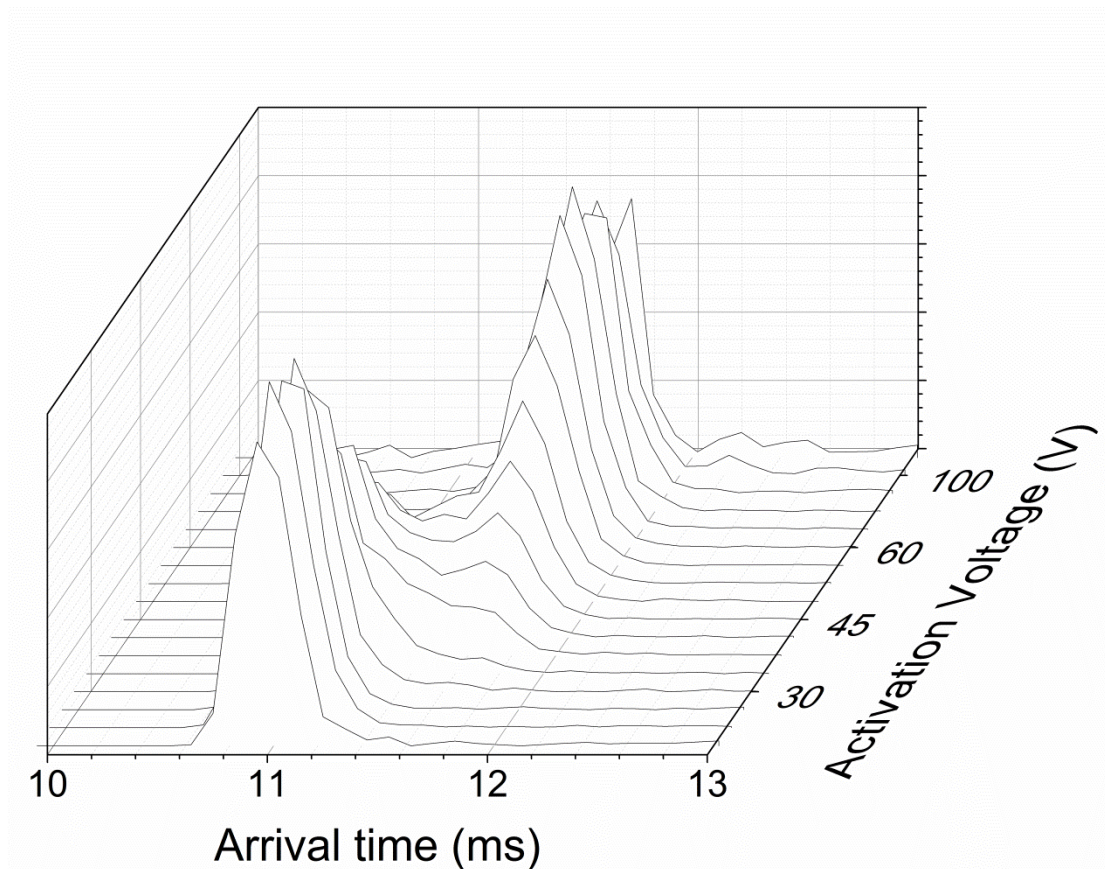


**Figure S- 5.** Plot of the evolution of the ATDs recorded after collisional activation of ion mobility selected  $cis$ -[Ru(bpy)<sub>2</sub>(DMSO)<sub>2</sub>]<sup>2+</sup> ions. The selection window was set to select only ions attributed to the SS isomer before activation. The signature of isomerization is visible through the apparition of ion signal at drift times corresponding to the SO and OO isomers as the collision voltage is increased.



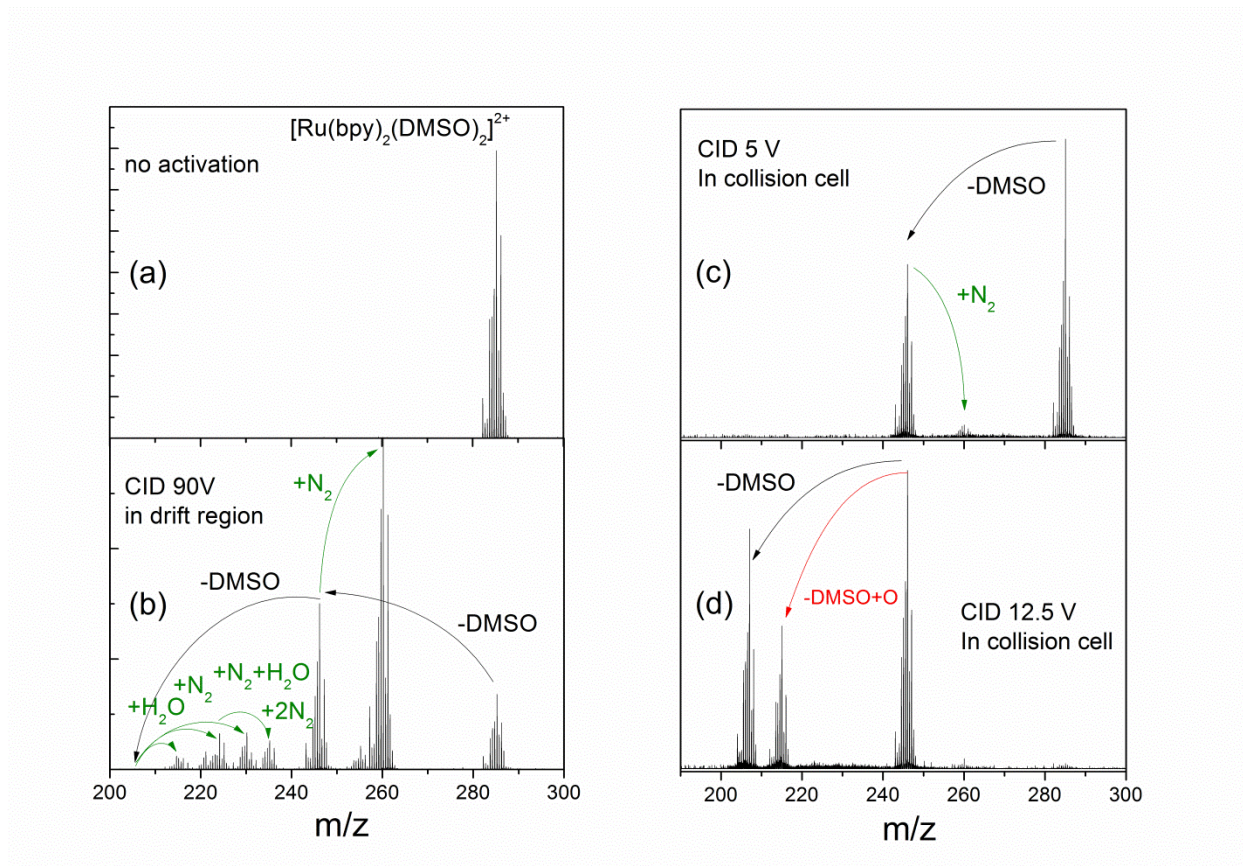


**Figure S- 6.** Mass spectra recorded for ion-mobility-selected  $[\text{Ru}(\text{bpy})_2(\text{DMSO})_2]^{2+}$  ions corresponding to the OO isomer. Without collisional activation (a), after 90 V collisional activation within the drift region (b), and after 5 V and 12.5 V collisional activation in the collision cell of the instrument, (c, and d, respectively). In all cases, the loss of DMSO is the main observed channel. The different species labelled in green in panel (b) are the result of the reactions of  $[\text{Ru}(\text{bpy})_2(\text{DMSO})]^{2+}$  and  $[\text{Ru}(\text{bpy})_2]^{2+}$  with  $\text{N}_2$  and water in the transfer region of the instrument, after separation, as illustrated in **Figure S- 7**.

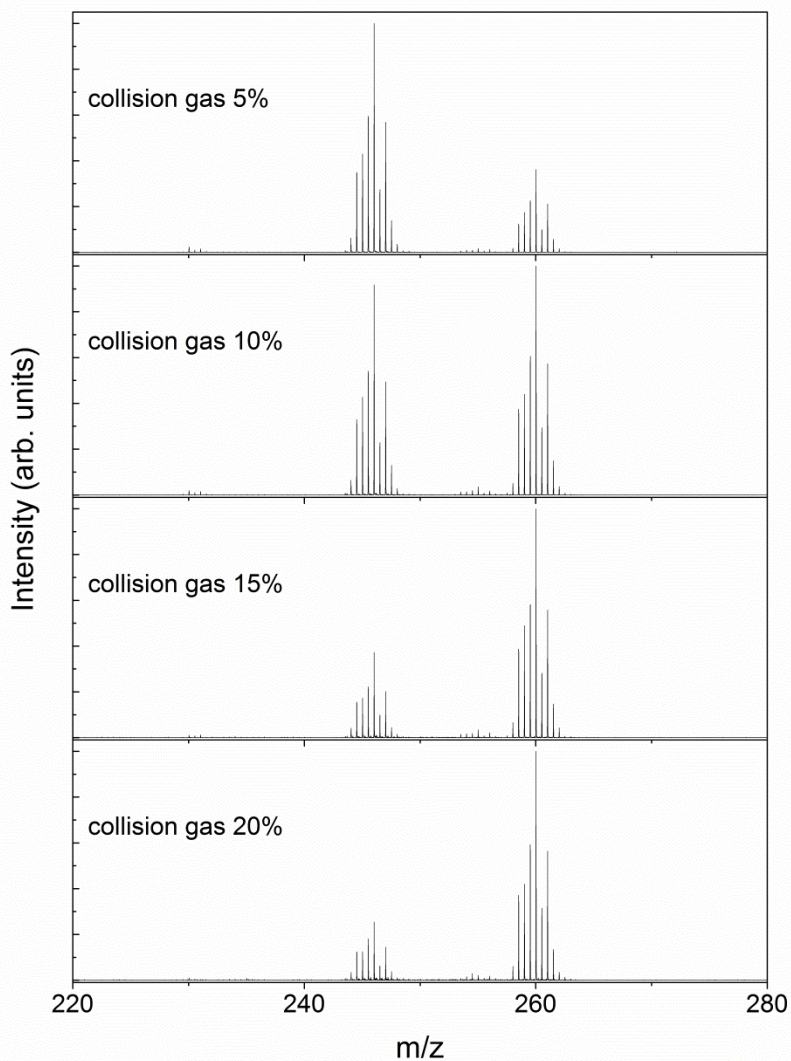


**Figure S- 7.** Mass spectra recorded for mass-selected  $[\text{Ru}(\text{bpy})_2(\text{DMSO})]^{2+}$  ions ( $m/z$  246 ) with different flows for the collision gas ( $\text{N}_2$ ) in the Bruker Maxis collision cell. The amount of ions at  $m/z$  260 ( $[\text{Ru}(\text{bpy})_2(\text{DMSO})+\text{N}_2]^{2+}$ ) increases with the collision gas pressure, indicating that they can be formed as a secondary product after dissociation of the initial complex. A small amount of water adducts ( $m/z$  255) is also visible.

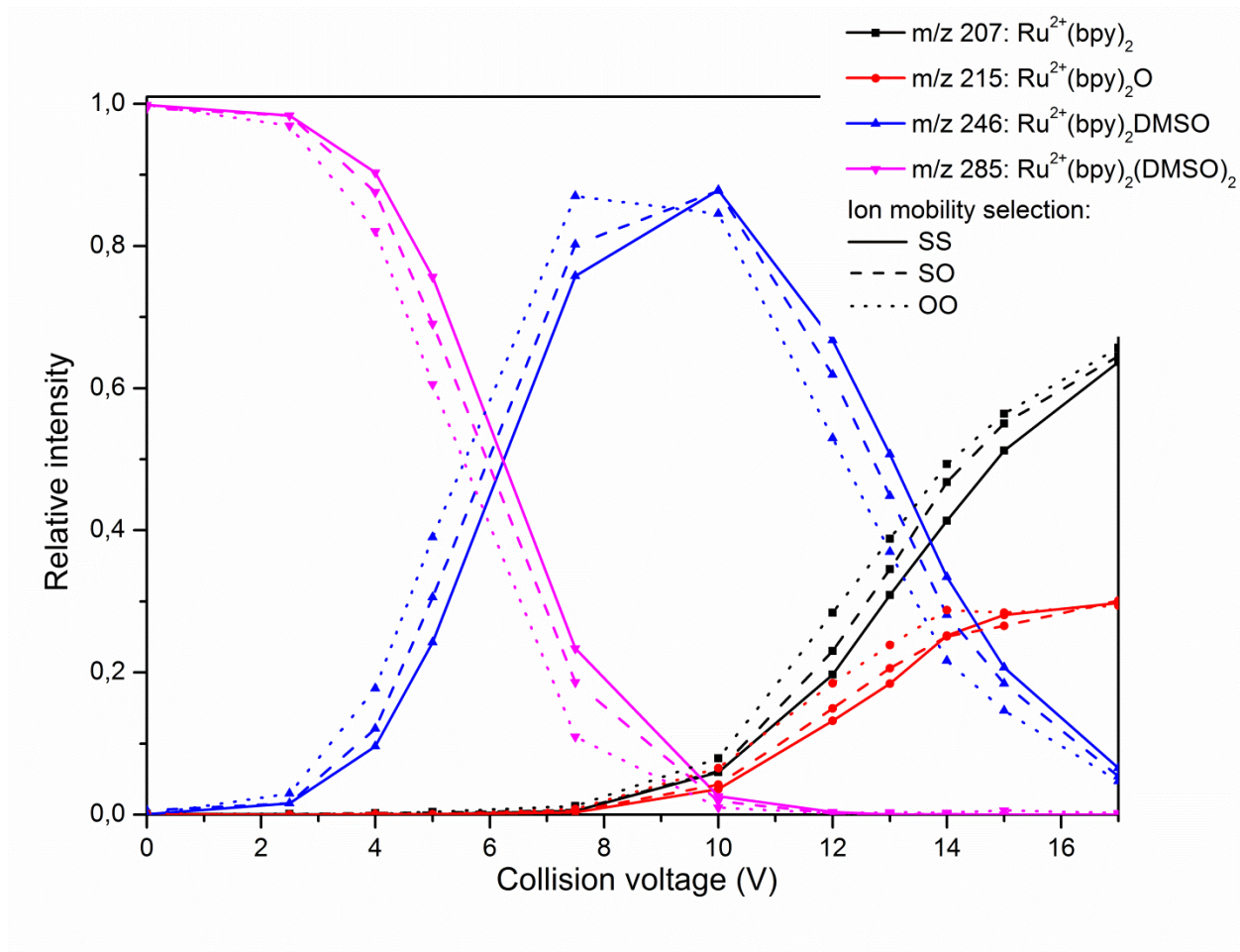


**Figure S- 8.** Relative intensities of the different products observed after collisional activation of mass- and ion mobility-selected *cis*-[Ru(bpy)<sub>2</sub>(DMSO)<sub>2</sub>]<sup>2+</sup> ions (m/z 285) in the collision cell of the instrument. Selecting different isomers before activation does not change the nature of the fragments, but changes the fragmentation yield.



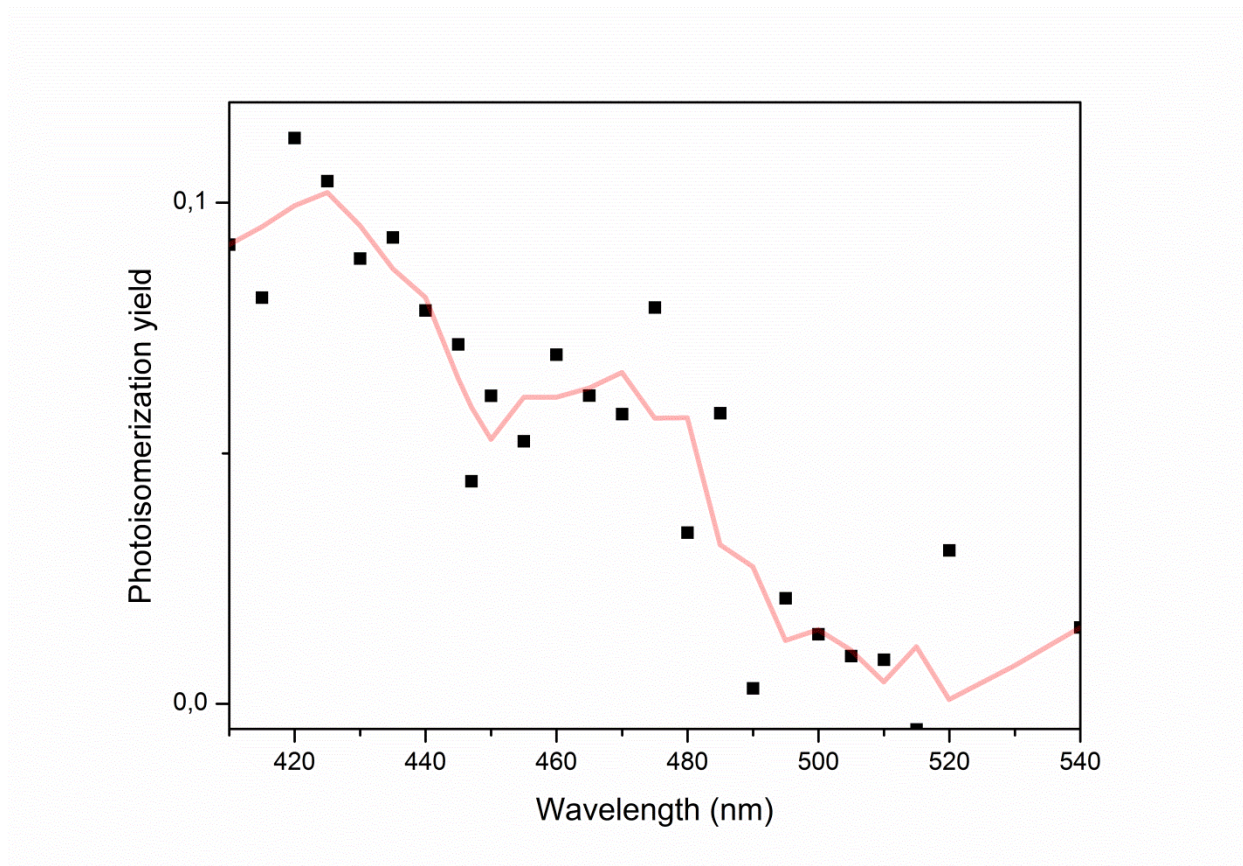


**Figure S- 9.** Photo-isomerization spectrum recorded for ion mobility selected  $[\text{Ru}(\text{bpy})_2(\text{DMSO})_2]^{2+}$  ions corresponding to the SO isomer. The black dots represent the photoisomerization yield for the SO $\rightarrow$ OO transition extracted from ATDs recorded after irradiation for 100 ms at different wavelength using a picosecond laser. The red line has been obtained by smoothing the experimental data and is provided to guide the eye.

## References

- (1) Mesleh, M. F.; Hunter, J. M.; Shvartsburg, A. A.; Schatz, G. C.; Jarrold, M. F. Structural Information from Ion Mobility Measurements: Effects of the Long-Range Potential. *J. Phys. Chem.* **1996**, *100* (96), 16082–16086.
- (2) Göttle, A. J.; Alary, F.; Dixon, I. M.; Heully, J.-L.; Boggio-Pasqua, M. Unravelling the S  $\rightarrow$  O Linkage Photoisomerization Mechanisms in Cis - and Trans - $[\text{Ru}(\text{bpy})_2(\text{DMSO})_2]^{2+}$  Using Density Functional Theory. *Inorg. Chem.* **2014**, *53* (13), 6752–6760.

- (3) Smith, M. K.; Gibson, J. A.; Young, C. G.; Broomhead, J. A.; Junk, P. C.; Keene, F. R. Photoinduced Ligand Isomerization in Dimethyl Sulfoxide Complexes of Ruthenium(II). *Eur. J. Inorg. Chem.* **2000**, 2000 (6), 1365–1370.